Ab initio approach of the hydrogen insertion effect on the magnetic properties of YFe_2

Valérie Paul-Boncour[1] and Samir F. Matar[2,*]

[1]*Laboratoire de Chimie Métallurgique des Terres Rares, CNRS, 2-8 rue H. Dunant, F-94320 Thiais Cedex, France*

[2]*Institut de Chimie de la Matière Condensée de Bordeaux, I.C.M.C.B-CNRS, Université Bordeaux 1, 87 avenue Docteur Albert Schweitzer, F-33608 Pessac Cedex, France*

(Received 12 May 2004; revised manuscript received 27 August 2004; published 24 November 2004)

Based on experimental crystallographic and magnetic results on the family of hydrides YFe_2H_x ($0<x\leqslant 5$) which point to a loss of magnetization for high H content, an assessment of the electronic, magnetic, and chemical bonding properties is provided within the local spin density functional theory using the augmented spherical wave method. The volume effect is analyzed for the hydrogen free alloy then with insertion of hydrogen. It is found to prevail up to ~3 H/fu with an increase of the magnetization due to enhanced localization of the Fe($3d$) orbitals. For $x_H \geqslant 4$ the chemical role of hydrogen becomes dominant over volume expansion effect and magnetization decreases; the absence of magnetic moments for YFe_2H_5 is explained based on prevailing Fe—H bonding.

DOI: 10.1103/PhysRevB.70.184435 PACS number(s): 71.15.Mb, 62.20.Qp, 71.20.−b, 79.20.Uv

I. INTRODUCTION

Binary alloys belonging to the Laves family AB_2 (A = rare earth or actinide, B = transition metal) crystallize either in a face centered cubic fcc lattice ($C15$) or in a hexagonal lattice ($C14$).[1] One of the basic aspects of the electronic properties of the pure AB_2 alloy systems is the identification of the origin of the magnetism which can be either due to the transition metal or induced by the A metal, depending on the chemical nature of the involved species.[2,3] Further, a particular interest arises from the capacity of these alloys to readily absorb hydrogen with almost continuous amounts ranging from 1.3 to 5 in RFe_2H_x (R=Y, Er) for instance.[4,5] Besides the large potential applications of the resulting hydrides, there is a basic interest in studying the magnetic structure and the electronic properties due to the H insertion. In the RFe_2H_x P-C_H-T (pressure-composition temperature) diagrams we have observed several equilibrium plateaus related to the existence of phases with different structures derived from the $C15$ lattice of the pristine RFe_2 system. The observed lowering of the crystal symmetry was found to be related to the ordering of hydrogen atoms in preferential interstitial sites. For five inserted H atoms, an orthorhombic symmetry with space group ($Pmn21$) was adopted by the hydride lattice.[5] The structure of the hydrogen rich phase is given in Fig. 1. The experimentally observed evolution of the magnetic properties of these systems exhibits an increase of the magnetization magnitude of Fe with the amount of absorbed hydrogen (i.e., up to 3.5 H per RFe_2 followed by a strong drop for 5 H per YFe_2 leading to a nearly paramagnetic behavior of Fe. The interplay of the volume versus chemical effects of hydrogen should be examined and addressed at a level involving the contribution of each atomic species. This can be done with help of computations within the well established framework of the density functional theory (DFT)[6,7] such as those we shall use here.

II. CRYSTAL AND MAGNETIC STRUCTURES OF YFE_2 AND YFE_2H_x

YFe_2 crystallizes in the cubic $C15$ type structure described in the $Fd\bar{3}m$ space group. It is ferromagnetic (see Sec. IV A 2) with Fe moment of $1.8\mu_B$ and a Curie temperature T_C=560 K. Hydrogen absorption into YFe_2 leads to the formation of hydrides YFe_2H_x with $1.3\leqslant x\leqslant 5$.[8–10,12] The main effect is a regular increase of the cell volume versus x accompanied by various structural distortions of the cubic lattice. This lowering of the crystal symmetry can be related to hydrogen order in preferential tetrahedral interstitial sites (A_2B_2 and AB_3).[9–11] These hydrides recover the cubic $C15$ structure through a first order transition above the temperature T_S (Fig. 2). This order-disorder transition temperature decreases as the hydrogen content increases as reported in Fig. 2 which is an extension to x=5 of Fig. 6 in Ref. 13. T_C first increases from 560 to 720 K (x=1.3), then decreases linearly down to 363 K for x=3.5 (Fig. 2). For x=4.2, the compound is ferromagnetic from 4.2 to 140 K, then there is a sharp decrease of the magnetization related to a decrease of the Fe moment and a rotation around the monoclinic b axis.[12] Above 140 K, the magnetization curves are strongly field dependent.[12,13] In addition this transition is very sensitive to the replacement of hydrogen by deuterium since in this case the transition occurs at 90 K instead of 140 K. For YFe_2H_5, which crystallizes in an orthorhombic structure [$Pmn21$ space group, a=5.437(1) Å, b=5.850(1) Å, and c=8.083(1) Å], there is no more ordered magnetic moment on the Fe site,[14] hence no Curie temperature. It is noticeable that in the YFe_2H_x system the structural and magnetic ordering temperatures are not correlated pointing out different origin of these transitions. Reporting on the composition dependence of the saturation magnetization and of the hyperfine fields, the results are displayed in Figs. 3(a) and 3(b). The magnetization measurements were carried out at 4.2 K under a magnetic field up to 200 kG in order to reach saturation. The evolution of the mean Fe hyperfine field versus H content shown in Fig. 3(b) is for measurements at 4.2 K using Mössbauer spectroscopy. Three regimes can be observed: (i) For $1.3\leqslant x\leqslant 3.5$ the hydrides display a progressive increase of the saturation magnetization [Fig. 3(a)] and of the mean hyperfine field on iron [Fig. 3(b)]; (ii) for x=4 there is a decrease of both M_S and B_{HF}, and (iii) for x=5 the saturation magnetization drops to less than $1\mu_B$ and the hyperfine field vanishes. The absence of hyperfine field down to 4.2 K indi-

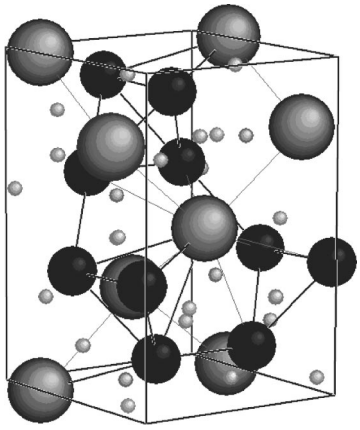

FIG. 1. Crystal lattice of the orthorhombic structure of YFe_2H_5. Large grey spheres, Y; black spheres, Fe; small grey spheres, H.

cates the absence of ordered Fe moment.[8] Nevertheless the observed remaining magnetization of $0.4\mu_B$/Fe can be explained by a paramagnetic state associated with large spin fluctuations, since we are close to the onset of ferromagnetism.

In order to understand the evolution of the Fe moment we have undertaken band structure calculations on the hydrogen free alloy system YFe_2 and on the hydrides. For the cubic *C*15 structure, the hydrogen sites were calculated with the assumption that they are located in A_2B_2 sites and that the distances between two H atoms are larger than or equal to 2.1 Å according to the Switendick criterion.[15] For orthorhombic YFe_2H_5, it is possible to use the site positions determined from the neutron diffraction study on isostructural $ErFe_2D_5$ (Ref. 5) (cf. Table I). For the purpose of getting full site filling we have selected the sites with the highest occupancy factor and set them to 1. The only problem is for two sites (*D*1 and *D*2) which are only half occupied since the distances between two of the atoms in these sites is shorter than 2.1 Å. To overcome this difficulty we have searched a lower symmetry which allows to split the sites with too small H—H distances into two different ones and let occupy only one of these two positions. This can be done in a monoclinic *P*1*n*1 space group which is a subgroup of orthorhombic *Pmn*21 group (see Table I). In this work hydrogen insertion effects within YFe_2 are examined within two complementary approaches relevant to (i) the influence of volume expansion on the magnetic properties within the *C*15 structure and the

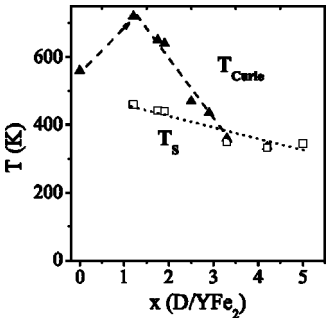

FIG. 2. Order temperature versus D content in YFe_2.

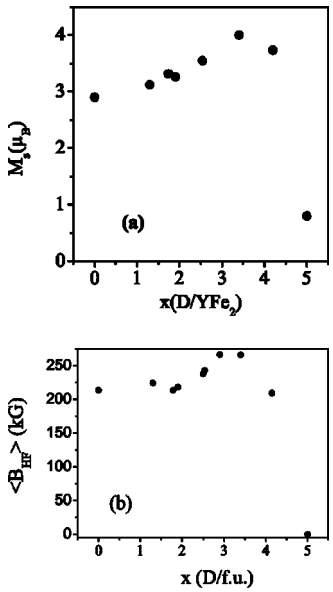

FIG. 3. Saturation magnetization (a) and hyperfine field B_{HF} (b) versus D content in YFe_2.

*Pmn*21 distorted lattice of YFe_2 alloy system and (ii) to the chemical role of hydrogen and its influence on the changes of the magnetization of the hydride lattice for increasing amounts of hydrogen for YFe_2H_3 in the cubic structure, YFe_2H_4 in the orthorhombic *Pmn*21 space group and YFe_2H_5 in monoclinic lattice symmetry.

III. COMPUTATIONAL FRAMEWORK

A. Electronic and magnetic properties

Among the self-consistent methods built within the DFT (see for instance Ref. 16) we use a scalar relativistic implementation of the augmented spherical wave (ASW) method[17–19] which can lead to an assigned role to each atomic species in the magnetism and in the bonding. The effects of exchange and correlation are accounted for within a local spin density approximation (LSDA) scheme.[20] All valence electrons were treated as band states. In the minimal ASW basis set,[18] we chose the outermost shells to represent the valence states and the matrix elements were constructed using partial waves up to $l_{max}+1=4$ for Y, $l_{max}+1=3$ for Fe, and $l_{max}+1=2$ for H. Besides its use of the LSDF (local spin density functional theory), the ASW method is based on the atomic sphere approximation (ASA) which assumes overlapping spheres centered on the atomic sites within which the potential has a spherical symmetry (central potential). The volume of the spheres must be equal to the cell volume because the wave equation is solved only in the spheres. This is unproblematic for closely packed structures like metals and intermetallics, but for loosely packed structures such as those of the hydrides we study here, empty spheres (ES) are introduced to represent the interstitial space and to avoid an otherwise too large overlap between the actual atomic spheres. ES are "pseudoatoms" with zero atomic number. They receive charges from the neighboring atomic species and allow for possible covalency effects within the lattice.

TABLE I. YFe_2H_x, description of the lattice parameters and atomic positions for the three different cells: cubic *C*15, orthorhombic, and monoclinic. Concerning the position of the D atom in the orthorhombic cell, only those which were found occupied and therefore refined have been reported.

	*C*15		*Pmn*21		*P*1*n*1	
Lattice	Cubic		Orthorhombic		Monoclinic	
Parameters	a (Å)		$a' \approx b' \approx * \sqrt{2}$ (Å)	$c' \approx c$ (Å)	a', b', c' (Å)	$\beta = 90°$
	8.011		$a' = 5.437$ $b' = 5.850$	$c' = 8.083$	$a' = 5.437$ $b' = 5.850$	$c' = 8.083$
Atom	Site	x,y,z	Site	x,y,z	Site	x,y,z
Y	8*a*	$\frac{1}{8},\frac{1}{8},\frac{1}{8}$	Y1:2*a*	0,0.262,0	Y1:2*a*	0,0.262,0
			Y2:2*a*	0,0.762,0.77	Y2:2*a*	0,0.762,0.77
Fe	16*d*	$\frac{1}{2},\frac{1}{2},\frac{1}{2}$	Fe1:4*b*	0.255,0.257,0.637	Fe1*a*:2*a*	0.255,0.257,0.637
					Fe1*b*:2*a*	0.745,0.257,0.637
			Fe2:2*a*	0,−.027,0.395	Fe2:2*a*	0,−0.027,0.395
			Fe3:2*a*	0,0.487,0.382	Fe3:2*a*	0,0.487,0.382
D (*A*2*B*2)	96*g*	x,x,z	D1:4*b*	0.04,0.235,0.273	*D*1*a*:2*a*	0.04,0.235,0.273
		$x=0.3368$			D1*b*:2*a*	0.96,0.235,0.273
		$z=0.1556$	D2:4*b*	0.428,0.28,0	D2*a*:2*a*	0.428,0.28,0.0
					D2*b*:2*a*	0.527,0.28,0.0
			D3:2*a*	0,0.388,0.719	D3:2*a*	0,0.388,0.719
			D4:2*a*	0,0.883,0.033	D4:2*a*	0,0.883,0.033
			D5:4*b*	0.214,0.580,0.953	D5*a*:2*a*	0.214,0.580,0.953
					D5*b*:2*a*	0.786,0.580,0.953
			D6:4*b*	0.270,0.930,0.304	D6*a*:2*a*	0.27,0.93,0.304
					D6*b*:2*a*	0.73,0.930,0.304
D (A*B*3)	32e	x,x,x	D7:2*a*	0,0.063,0.588	D7:2*a*	0,0.063,0.588
		$x=0.7118$	D8:2*a*	0,0.57,0.178	D8:2*a*	0,0.57,0.178

B. Chemical bonding properties

The results obtained from LSDF calculations are quite relevant for the magnitudes of the magnetic moments, the nature and energy position of the states with respect to the Fermi level, etc. However a more elaborate tool is needed to obtain information about the nature of the interaction between atomic constituents as well as the respective quantum states involved. This can be provided using overlap population (OP) leading to the so-called COOP (crystal orbital overlap population)[21] or alternatively introducing the Hamiltonian based population COHP (crystal orbital Hamiltonian population).[22] Both approaches provide a qualitative description of the chemical interactions between two atomic species by assigning a bonding, nonbonding or antibonding character. A slight refinement of the COHP was recently proposed in the form of the "covalent bond energy" E_{COV} which combines both COHP and COOP so as to make the resulting quantity independent of the choice of the zero of potential.[23] The E_{COV} was recently implemented within the ASW method.[24] Our preliminary experience with both COOP and E_{COV} shows that they give similar general trends although COOP exagerate the magnitude of antibonding states. We shall be using the E_{COV} description of the chemical bond in this work.

IV. RESULTS AND DISCUSSION

A. YFe_2 versus volume and distortion effects

1. Electronic structure and chemical bonding properties

In order to assess volume effects within YFe_2, calculations were carried out at the experimental and expanded cell volume of the *C*15 $Fd\bar{3}m$ type structure. For our choice of the atomic spheres radii, $r_{\mathrm{Y}}/r_{\mathrm{Fe}} = 1.22$, minimizing the overlap between the atomic spheres in the ASA, very little charge transfer could be observed between the different species. Testing other radii did not change this result significantly. Hence it can be argued that the bonding is not mainly due to charge transfer but rather imposed by the hybridization between the different valence states.

The derived lattice constant from the hydride was 8.14 Å; the experimental lattice constant being 7.35 Å. Further, assuming the orthorhombic *Pmn*21 space group of YFe_2H_5 (Ref. 5) another calculation was done with the actual hydride orthorhombic lattice constants given in Table I. These calculations are meant to simulate both the volume and structure distortion effects brought by the insertion of hydrogen.

At self-consistent convergence using a high precision integration of the fcc-first Brillouin zone, charge transfer (for instance within *C*15 YFe_2 at experimental lattice spacing)

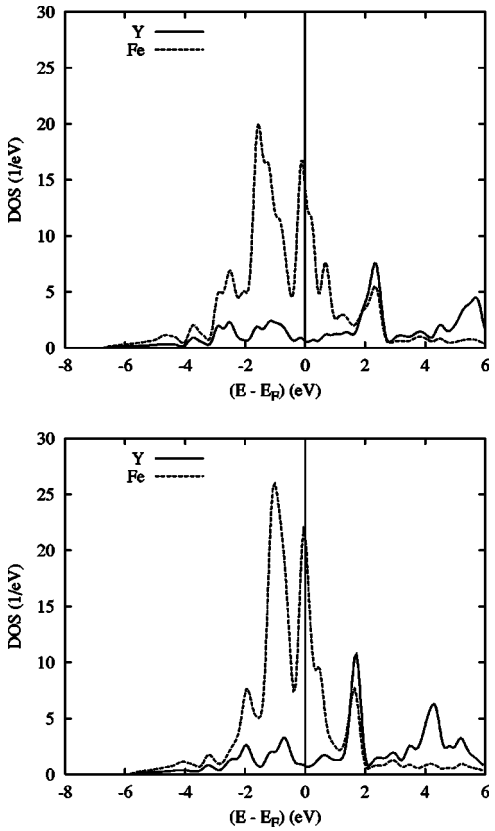

FIG. 4. Nonmagnetic site projected DOS of YFe_2 in the $C15$ structure at experimental (top) and expanded (botton) lattice volumes.

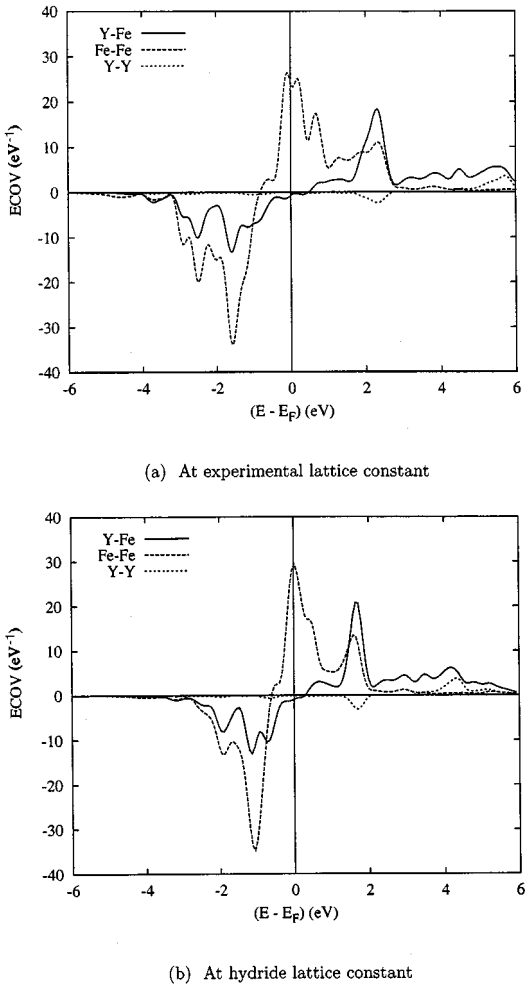

FIG. 5. Y-Fe, Fe-Fe, and Y-Y pair interactions in $C15$ YFe_2 at the experimental (top) and expanded (bottom) lattice volumes.

shows a departure of 0.35 electron from Y spheres to Fe spheres. This slight transfer, not significant of ionic effects—rarely observed in the framework of such *ab initio* calculations—signals a redistribution of the two *s* electrons of yttrium over its three valence basis sets thus providing it with a *d* character arising from its mixing with Fe($3d$). Therefore one can conclude that the major effect is that of the hybridization of the different valence states, not the charge transfer.

The site projected DOS for an assumed nonmagnetic ground state (nonspin polarized NSP) accounting for site multiplicity (twice more Fe than Y) are shown in Fig. 4 for the $C15$ YFe_2 lattice at the experimental as well as at the hydride lattice parameters. The origin of energies along the *x* axis is taken with respect to the Fermi energy; this is equally followed in all other plots. Looking first at the general shape of the DOS one can observe the predominance of the Fe states in the close neighborhood of the Fermi level (E_F), i.e., with respect to very low intensity yttrium states. The major effect of a larger lattice spacing can be seen from the narrower states within the valence band and the increase of the DOS magnitude at the Fermi level $n(E_F)$ from 15 to 20 eV^{-1}. The similar skylines between the partial DOS pointing to the mixing between Fe and Y states can be seen at the lower part of the valence band (VB), with mainly *sp* like states between −6 and −2 eV, as well as toward the top of VB (*d* states). Such mixing will be further analyzed in the next paragraph regarding the chemical bonding. Last, within the conduction band (CB), Y($4f$) states are found dominant as it can be expected from their emptiness. Similar DOS features to Fig. 4 are obtained for the expanded YFe_2 lattice in the orthorhombic structure of the hydride so that their discussion follows from above and they are not shown here.

The analysis of the chemical bonding is done using the E_{COV} approach presented above. The corresponding plots are shown in Fig. 5; we do not show the E_{COV} plots for the orthorhombic YFe_2 expanded lattice which look like those of the expanded lattice in $C15$ symmetry. Along the coordinate axis negative, positive, and zero E_{COV} magnitudes (in eV^{-1}) point to bonding, antibonding, and nonbonding states, respectively. Partial E_{COV} are given for the interactions of total species of each lattice type for the Y-Fe, Fe-Fe, and Y-Y bonds. The Y-Y interaction is found to be the lowest in magnitude. On the contrary the magnitude of the Fe-Fe interaction is found to be dominant within the valence band as well as above the Fermi level although it is qualitatively lower when the lattice is expanded pointing to smaller overlap between the atomic orbitals. This should have consequences on a larger magnitude of the atomic moment carried by Fe within the expanded lattice as it will be shown in the

next section. The antibonding character of the Fe-Fe interaction towards the top of the valence band and at E_F points to the instability of the system in the nonmagnetic NSP configuration. On the contrary, due to the lower occupation of yttrium states, its interaction with Fe as well as with the other Y atom gives bonding states up to E_F and beyond within the conduction band; this Y-Fe bonding largely contributes to the stability of the system. The sharp peak at ~2eV corresponds to Fe(d)-Y($4f$) interactions. The electrons in the d band crossed by the Fermi level are not all antibonding meaning that there is a part of them which becomes nonbonding in the neighbourhood of E_F and participate to the onset of the magnetic moment as it is discussed in the next section.

2. Magnetic properties

As it can be expected for the magnetic configuration of YFe_2 at the experimental lattice constant, there is an energy stabilization of $\Delta E \sim 0.95$ eV per unit cell with respect to the NSP calculation. The magnetic moments are $M(\mathrm{Y}) = -0.50\mu_B$ and $M(\mathrm{Fe}) = 1.85\mu_B$ with a total magnetization $M_{\mathrm{cell}}^{\mathrm{calc}} = 6.37\mu_B$, i.e., $3.18\mu_B$ per formula unit. This value is close to the one found experimentally, $M_{\mathrm{YFe_2}}^{\mathrm{exp}} = 2.9\mu_B$ (Ref. 25) and to the calculated value by Mohn and Schwarz.[26] From this YFe_2 is a ferrimagnet in its ground state, contrary to certain experimental results which announce it as a ferromagnet with a zero moment on yttrium.[25] Another significant result that we extract from these calculations is the Fermi contact term of the hyperfine field (H_{FC}) based on the spin density at the nucleus for the *ns* quantum states caused by the polarization of the *s* electrons by the *d* moments: $H_{\mathrm{FC}}^{\mathrm{calc}}(\mathrm{Fe}) = -250$ kGauss. The experimental value $H_{\mathrm{FC}}^{\mathrm{exp}}(\mathrm{Fe}) = -220$ kGauss (Ref. 25) points to a good agreement and comforts the computed electronic structure. The expanded lattice of the alloy at the YFe_2H_5 volume shows an enhanced magnitude of the moments for both constituents, $M(\mathrm{Y}) - 0.81\mu_B$ and $M(\mathrm{Fe}) = 2.42\mu_B$ with a total magnetization $M_{\mathrm{cell}}^{\mathrm{expand}} = 8.08\mu_B$, i.e., $4.04\mu_B$ per formula unit.

These magnetization results are illustrated by the site projected SP-DOS plotted in Fig. 6 which can help to further assess them. A general trend is that the weights of the DOS at ↑ and ↓ spin populations are not the same meaning that it is not a rigid band shift which rules the magnetism of this system like in αFe but it is rather that of a covalent magnetism formerly shown for $ZrFe_2$.[26] The consequence is that the moment of yttrium is provided by the covalent Y-Fe bond rather than by a rigid energy shift of nonmagnetic DOS, whence its negative sign—notice the Y-Fe overlap around −1 eV for ↓ DOS. Beside the energy shift between the two spin populations causing the onset of the magnetic moment, there can be seen an enhanced localization of the Fe states (sharper DOS peaks, less Fe-Fe overlap) for the expanded cell which explains the larger moment magnitudes.

Last the effect of lattice distortion of YFe_2 in the orthorhombic *Pmn*21 space group leads to closely the same magnitude of the magnetization, $M_{\mathrm{cell}}^{\mathrm{expand\text{-}distorted}} = 16.45\mu_B$, i.e., M $4.11\mu_B$ per formula unit with the following distribution of the atomic moments over the twofold Y and threefold Fe lattice sites: $M(\mathrm{Y}) = -0.721/-0.724$ and $M(\mathrm{Fe}) = 2.44/2.39/2.39\mu_B$. The agreement with the *C*15 expanded YFe_2 results above points to a driving effect of the volume as with respect to the distortion one. Note that the increase of magnetic moment by volume expansion was also observed recently by first principal calculations in YFe_2H_4.[27]

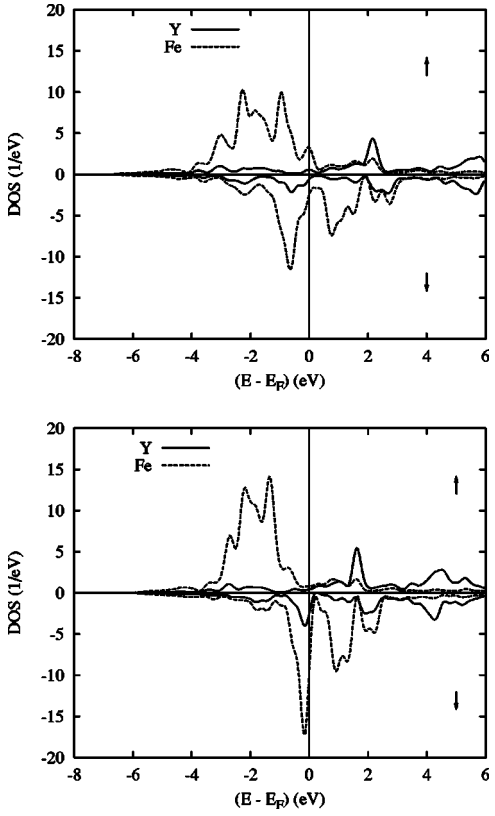

FIG. 6. Spin polarized site projected DOS of YFe_2 in the *C*15 structure at experimental (top) and expanded (bottom) lattice volumes.

B. YFe_2 and hydrogen effects

For the model structures accounting for the insertion of hydrogen within the YFe_2 lattice in ordered manner we have followed experimental findings regarding lattice expansions and distortions. Three different structural setups were assumed at increasing concentrations of hydrogen. The uppermost H content in *A*2*B*2 (96*g*) sites in *C*15 structure avoiding too small H-H distances ($d_{\mathrm{H\text{-}H}} \geqslant 2.1$ Å) (Ref. 15) is 3, i.e., YFe_2H_3. Then in the *Pmn*21 orthorhombic distorted lattice we considered YFe_2H_4 and last the monoclinic *P*1*n*1 structure was used for the hydrogen rich hydride YFe_2H_5 (Table II). Calculations were carried out for the magnetic spin polarized (SP) configuration using the experimental lattice constants; for the YFe_2H_4 intermediate H concentration composition the calculations were carried out at a volume computed in between those of YFe_2H_3 and YFe_2H_5.[4,5,8] In all systems we observe charge transfer to occur from the atomic species (Y, Fe, and H) to the empty spheres ES introduced in the framework of the ASA on which the ASW method is based. Its small amount of ~±0.2 electron per ES/atomic

TABLE II. YFe_2H_5, experimental and calculated positions in the $P1n1$ space group; (x,y,z), reduced atomic positions; N_{ref}, refined occupation numbers; N_{calc}=calculated occupation numbers.

Site	Atom	x	y	z	N_{ref}	N_{calc}
Y1	Y	0	0.2528	0	1	1
Y2	Y	0	0.7670	0.7777	1	1
Fe1*a*	Fe	0.2538	0.2536	0.6434	1	1
Fe1*b*	Fe	0.7462	0.2530	0.6450	1	1
Fe2	Fe	0	−0.0270	0.3997	1	1
Fe3	Fe	0	0.4840	0.3867	1	1
D1*a*	D	0.0623	0.2460	0.2762	0.5	0
D1*b*	D	−0.0583	0.2370	0.2796	0.63	1
D2*a*	D	0.4494	0.2980	0.0136	0.12	0
D2*b*	D	−0.4524	0.2980	0.0136	0.67	1
D3	D	0	0.3747	0.7272	1	1
D4	D	0	0.9070	0.0493	0.785	1
D5*a*	D	0.2109	0.5900	0.9595	1	1
D5*b*	D	−0.2098	0.5896	0.9595	1	1
D6*a*	D	0.2629	0.9394	0.3118	1	1
D6*b*	D	−0.2629	0.9394	0.3118	0.44	1
D7	D	0	0.0758	0.5916	0.99	1
D8	D	0	0.5580	0.1763	0.87	1
N(D)					9	10
D/fu					4.5	5

species points to the covalent character of the chemical bonding. This will be further explicited in next sections.

1. YFe_2H_3

The spin polarized calculations for the $C15$ YFe_2H_3 hydride give a magnetization per YFe_2 formula unit: $M=3.8\mu_B$ in agreement with experiment ($3.9\mu_B$), cf. Fig. 3 and with previous *ab initio* investigations by us on that system.[28] This magnetization enhancement is mainly driven by the increase of the moment carried by iron ($2\mu_B$ versus $1.85\mu_B$ in the alloy system) which equally leads to an increase of the absolute value of the Fermi contact term of the hyperfine field $H_{FC}=-232$ kGauss. Despite this result which favors the volume effect of hydrogen (larger localization of the DOS similarly to the expanded alloy system, see Fig. 4), the onset of an Fe-H chemical bonding significantly larger than the Y-Fe one partly due to the shorter average Fe-H distance, was pointed out.[28] This is further developed for hydrogen rich systems YFe_2H_4 and YFe_2H_5 hereafter.

2. YFe_2H_4 and YFe_2H_5

At self-consistency the magnetization of YFe_2H_4: $M=3.35\mu_B$ per formula unit is found to be slightly smaller than that of YFe_2H_3. This is due to the decrease of the fourfold Fe($4b$) moment ($1.48\mu_B$) as with respect to the two twofold Fe($2a$) moments (2.22 and $2.46\mu_B$, respectively) which arise from the changes of the Fe-H distances computed as largest for the Fe($2a$) sites (Table I), 1.72 Å. This leads to a lower average Fe moment of $\sim 1.9\mu_B$. On the contrary the calculation of the magnetic structure of monoclinic YFe_2H_5 gives a vanishing magnetization with no polarization of the atomic species. Although this agrees with the experimental curve $\sigma_s=f(x_D)$ in Fig. 3, an assessment is orderly with the help of the DOS and E_{COV} plots.

Figure 7 gives the SP DOS of the two systems YFe_2H_4 and YFe_2H_5. The projected density of states of the different crystallographic sites are gathered for each atomic species to make the presentation clear (i.e., we do not show the splitting effects into the different crystallographic sites in the orthorhombic and monoclinic distortions). Although they show a large contribution in the lower part of the valence band, hydrogen states are found in a broad energy range of the DOS; furthermore they show a similar skyline to the Fe (as well as Y) DOS. This feature should be further assessed by the analysis of the chemical bonding in the next section. The largest contribution to the DOS arises from Fe states. While spin polarization causes energy shift between majority ($\uparrow$) and minority ($\downarrow$) spin states within YFe_2H_4, there is no energy shift for the YFe_2H_5 in agreement with the absence of magnetization. The other feature we mention is the splitting of the DOS into massifs whose isolation with respect to each other can be seen most pronounced for YFe_2H_5, *s*-like from -10 to ~ -7.5 eV, *sp*-like $[-7,-3$ eV], Fe(d)-t_{2g}-like $[-3,0.5$ eV], and Fe(d)-e_g-like $[0.5,\sim 3$ eV] together with Y($4f$) empty states within the CB. This could point to the increasing ioniclike behavior of the hydrogen-rich system.

3. Discussion of the chemical bonding

Figure 8 shows chemical bonding features for the spin $\uparrow$ and $\downarrow$ channels for pair interactions of metal-metal (Y-Fe,

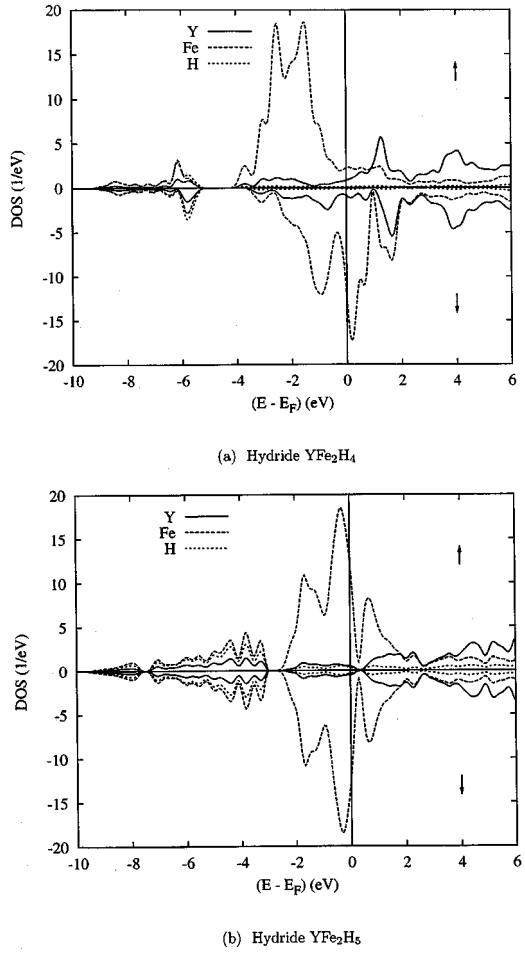

FIG. 7. Spin polarized DOS of hydrogen rich hydrides YFe_2H_4 and YFe_2H_5.

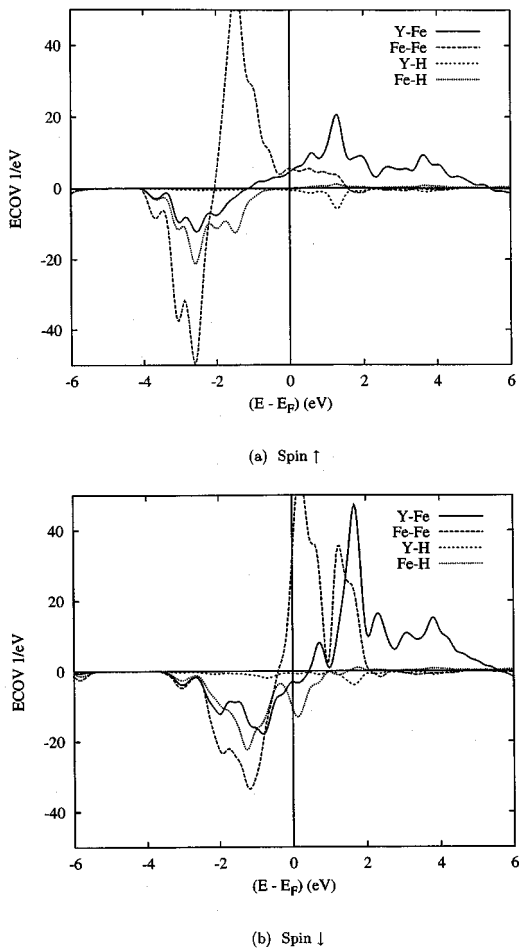

FIG. 8. Spin resolved chemical bonding properties of YFe_2H_4 for metal-metal and metal-hydrogen pair intercations.

Fe-Fe) and metal-hydrogen (Y-H, Fe-H) bonds. Due to the lowering of the lattice symmetry from cubic to orthorhombic, the plots regroup for each chemical species the crystallographic sites contributions with their multplicities. The overall energy shift within the valence band follows the common SP-DOS feature in itinerant magnetism of the stabilization for majority spins (↑) and destabilization of minority spins (↓). All contributions but Fe-Fe show mainly bonding E_{COV} magnitudes within the valence band, the bonding contribution arising from Fe-H interaction can be seen to have similar magnitude to Y-Fe which points to their participation to the stability of the crystal lattice of the hydride. Turning to Fe states which are mainly affected by spin polarization, they exhibit Fe-Fe interactions which are half-bonding–half-antibonding within the spin ↑ valence band while the antibonding spin ↓ Fe-Fe interactions are found above the Fermi level. These results lead to propose an overall bonding of the lattice ensured by the Y-Fe and Fe-H interaction within both spin channels and ↓ Fe-Fe interactions. Due to the absence of spin polarization within monoclinic YFe_2H_5 pair interactions within majority and minority spins exhibits identical contributions so that Fig. 9 shows the chemical bonding for one of the two spin channels. Similar features to Fig. 8 are observed as to the relatively larger magnitude of Fe-H versus Y-Fe bonding as well as for the Fe-Fe interaction which is half-bonding–half-antibonding within the valence band. Further Fe-Fe and Y-Fe interactions have similar features to those discussed above for the alloy system (Fig. 5). There is a larger bonding with hydrogen as with respect to Fig. 8 which appears in the lower part of the valence band $[-6,-4$ eV]. Further Fe-H interaction becomes as large as Fe-Fe one and the antibonding contribution from

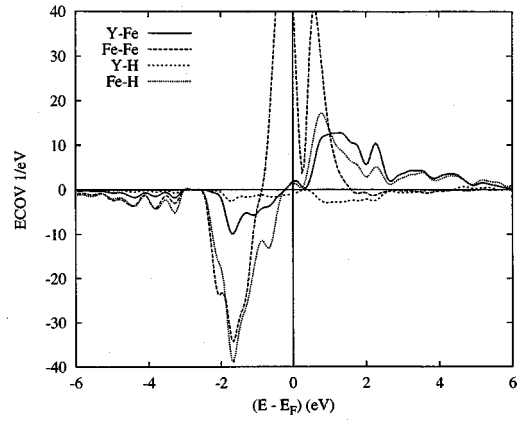

FIG. 9. Chemical bonding properties of YFe_2H_5 for metal-metal and metal-hydrogen pair interactions.

Fe-Fe drops to a minimum at the Fermi level, this is opposed to the large E_{COV} at E_F observed in the alloy system calculated in the nonmagnetic state (Fig. 5). From this the bonding of Fe-H can be seen to prevail when hydrogen is inserted within YFe_2 system at increasing amounts. The underlying mechanism is that of spin pairing of Fe with H leading to a progressive loss of the Fe moment. We underlined this feature in former calculations on iron nitride systems such as Fe_xN $(8 \leqslant x \leqslant 2)$.[29]

It can be noted here that the growing contribution of the Fe-H bonding relative to the Fe-Fe bonding as the hydrogen content increases can also be observed on the evolution of the Curie temperature T_C (Fig. 2) which reflects the modification of the Fe-Fe interactions. The first increase of T_C from $x=0$ to 1.3 can be explained by the dominant volumetric effect which reinforces the Fe-Fe interactions. Then the linear decrease of T_C from $x=1.3$ to 3.5 shows clearly that the additional Fe-H bonding progressively weakens the Fe-Fe interactions.

V. CONCLUSIONS

Based on experimental crystallography and magnetic measurements results on hydrides with technological importance, the aim of this work was to provide a band theoretical analysis within the local spin density functional theory of the volume versus chemical effect induced by hydrogen within the YFe_2 Laves alloy system. The volume effect is found to prevail up to ~3 H/fu leading to an increase of the moment of iron due to a larger localization of the 3*d* orbitals (site projected DOS analysis). For hydrogen rich systems (i.e., with 4 H/fu) the chemical role of hydrogen becomes important and at the YFe_2H_5 composition the magnetization vanishes with a dominant Fe-H bond. These findings which agree with experiment provide an atomic resolved electronic and magnetic analysis of the complex role of hydrogen.

ACKNOWLEDGMENTS

The authors wish to thank Dr. Volker EYERT from the University of Augsburg for a critical reading of the paper. Computational facilities provided within the intensive numerical simulation facilities network M3PEC of the University Bordeaux 1, partly financed by the Conseil Régional d'Aquitaine are acknowledged.

*Corresponding author. Electronic address: matar@icmcb-bordeaux.cnrs.fr

[1] F. Laves, *Theory of Alloy Phases* (American Society for Metals, Cleveland, OH, 1956), p. 124.
[2] A.M. Boring, R.C. Albers, G.H. Schadler, A.C. Lawson, P. Weinberger, and N.E. Christensen, Phys. Rev. B **36**, 5507 (1987).
[3] T. Konishi, K. Mamiya, K. Morikawa, K. Kobayashi, T. Mizokawa, A. Fujimori, F. Iga, H. Kawanaka, Y. Nishihara, A. Delin, and O. Eriksson, J. Electron Spectrosc. Relat. Phenom. **88**, 303 (1998).
[4] V. Paul-Boncour, L. Guénée, M. Latroche, M. Escorne, A. Percheron-Guégan, Ch. Reichl, and G. Wiesinger, J. Alloys Compd. **253–254**, 272 (1997).
[5] V. Paul-Boncour, L. Guénée, M. Latroche, A. Percheron-Guégan, B. Ouladdiaf, and F. Bourée-Vigneron, J. Solid State Chem. **142**, 120 (1999).
[6] P. Hohenberg and W. Kohn, Phys. Rev. **136**, B864 (1964).
[7] W. Kohn and L.J. Sham, Phys. Rev. **140**, 1133 (1965).
[8] V. Paul-Boncour, S.M. Filipek, I. Marchuk, G. André, F. Bourée, G. Wiesinger, and A. Percheron-Guégan, J. Phys.: Condens. Matter **15**, 4349 (2003).
[9] V. Paul-Boncour, M. Escorne, A. Mauger, M. Latroche, and A. Percheron-Guégan, J. Appl. Phys. **79**, 4253 (1996).
[10] V. Paul-Boncour, L. Guénée, M. Latroche, and A. Percheron-Guégan, J. Alloys Compd. **255**, 195 (1997).
[11] V. Paul-Boncour, L. Guénée, M. Latroche, A. Percheron-Guégan, B. Ouladdiaf, and F. Bourée-Vigneron, J. Solid State Chem. **142**, 120 (1999).
[12] V. Paul-Boncour, G. André, F. Bourée, M. Guillot, G. Wiesinger, and A. Percheron-Guégan, Physica B **350**, E27 (2004).
[13] V. Paul-Boncour and A. Percheron-Guégan, J. Alloys Compd. **293–295**, 237 (1999).
[14] V. Paul-Boncour, S.M. Filipek, A. Percheron-Guégan, I. Marchuk, and J. Pielaszek, J. Alloys Compd. **317–318**, 83 (2001).
[15] A.E. Switendick, Z. Phys. Chem., Neue Folge **117**, 89 (1979).
[16] J. Kübler and V. Eyert, "Electronic structure calculations," in *Materials Science and Technology*, Vol. 3A: Electronic and Magnetic Properties of Metals and Ceramics, Part I, edited by K. H.J. Buschow (VCH Verlag, Weinheim, 1992) pp. 1–145.
[17] A.R. Williams, J. Kübler, and C.D. Gelatt, Jr., Phys. Rev. B **19**, 6094 (1979).
[18] V. Eyert, "Electronic structure calculations for crystalline materials" in *Density Functional Methods: Applications in Chemistry and Materials Science*, edited by M. Springborg (Wiley, Chichester, 1997), pp. 233–304.
[19] D.D. Kölling and B.N. Harmon, J. Chem. Phys. **10**, 3107 (1977).
[20] J. von Barth and D.J. Hedin, J. Phys. C **5**, 1629 (1972); J.F. Janak, Solid State Commun. **25**, 53 (1978); S.H. Vosko, L. Wilk and M. Nusair, Can. J. Phys. **58**, 1200 (1980).
[21] R. Hoffmann, Angew. Chem., Int. Ed. Engl. **26**, 846 (1987).
[22] R. Dronskowski and P.E. Blöchl, J. Phys. Chem. **97**, 8617 (1993).
[23] G. Bester and M. FÄhnle, J. Phys.: Condens. Matter **13**, 11541 (2001).
[24] V. Eyert (unpublished).
[25] D.G. Westlake, J. Less-Common Met. **75**, 177 (1980).
[26] P. Mohn and K. Schwarz, Physica B & C **130**, 26 (1985).
[27] D.J. Singh and M. Gupta, Phys. Rev. B **69**, 132403 (2004).
[28] S.F. Matar and V. Paul-Boncour, C.R. Acad. Sci., Ser. IIc: Chim **3**, 27 (2000).
[29] S.F. Matar, J. Alloys Compd. **345**, 72 (2002).